Tomography and imaging at the PSICHE beam line of the SOLEIL synchrotron

A. King, N. Guignot, P. Zerbino, E. Boulard, K. Desjardins, M. Bordessoule, N. Leclerq, S. Le, G. Renaud, M. Cerato, M. Bornert, N. Lenoir, S. Delzon, J.-P. Perrillat, Y. Legodec, and J.-P. Itié

Citation: Review of Scientific Instruments **87**, 093704 (2016); doi: 10.1063/1.4961365
View online: http://dx.doi.org/10.1063/1.4961365
View Table of Contents: http://scitation.aip.org/content/aip/journal/rsi/87/9?ver=pdfcov
Published by the AIP Publishing

REVIEW OF SCIENTIFIC INSTRUMENTS **87**, 093704 (2016)

Tomography and imaging at the PSICHE beam line of the SOLEIL synchrotron

A. King,[1] N. Guignot,[1] P. Zerbino,[1] E. Boulard,[1] K. Desjardins,[1] M. Bordessoule,[1] N. Leclerq,[1] S. Le,[1] G. Renaud,[1] M. Cerato,[1] M. Bornert,[2] N. Lenoir,[3] S. Delzon,[4] J.-P. Perrillat,[5] Y. Legodec,[6] and J.-P. Itié[1]
[1]*Synchrotron SOLEIL, St-Aubin 91192, France*
[2]*Navier Laboratory UMR8205, Ecole des Ponts ParisTech, Paris, France*
[3]*PLACAMAT UMS3626, University of Bordeaux, Bordeaux, France*
[4]*UMR Biodiversité Gènes et Communautés, INRA, Bordeaux, France*
[5]*Laboratoire de Geologie de Lyon, Terre Planetes Environnement, UMR5276-CNRS-ENSLyon-UCBLyon1, Lyon, France*
[6]*IMPMC, UMPC, Paris, France*

(Received 17 December 2015; accepted 5 August 2016; published online 12 September 2016)

PSICHE (Pressure, Structure and Imaging by Contrast at High Energy) is the high-energy beam line of the SOLEIL synchrotron. The beam line is designed to study samples at extreme pressures, using diffraction, and to perform imaging and tomography for materials science and other diverse applications. This paper presents the tomograph and the use of the beam line for imaging, with emphasis on developments made with respect to existing instruments. Of particular note are the high load capacity rotation stage with free central aperture for installing large or complex samples and sample environments, x-ray mirror and filter optics for pink beam imaging, and multiple options for combining imaging and diffraction measurement. We describe how x-ray imaging techniques have been integrated into high-pressure experiments. The design and the specifications of the beam line are described, and several case studies drawn from the first user experiments are presented. *Published by AIP Publishing.* [http://dx.doi.org/10.1063/1.4961365]

I. INTRODUCTION

X-ray computed tomography (CT) is an imaging technique in which the internal structure of a sample can be reconstructed, non-destructively, in three dimensions. Parallel beam tomography has developed into one of the important applications of third generation synchrotron sources (Wang *et al.*, 2001; Stampanoni *et al.*, 2006; Uesugi *et al.*, 2009; Boller *et al.*, 2010; Maire and Withers, 2014; and Drakopoulos *et al.*, 2015). The high flux and coherence of such sources allow many different systems to be studied. Depending on the acquisition strategy and the algorithms used, the quantity reconstructed is either the local x-ray attenuation coefficient (absorption contrast) or the electron density (phase contrast) (Cloetens *et al.*, 1997; Cloetens *et al.*, 2006; Paganin *et al.*, 2002; Langer *et al.*, 2008; and Boller *et al.*, 2010). The high flux allows good quality measurements to be made quickly (<0.1 s/volume (Maire and Withers, 2014 and Lhuissier *et al.*, 2012)), or sub-nanosecond per radiograph (Rack *et al.*, 2014), which allows *in situ* studies of evolving systems, exploiting the non-destructive character of the technique. Alternatively, the non-destructive nature of the technique has made it an important tool for the study of unique samples, such as fossils or cultural artifacts (Bertrand *et al.*, 2012). Recent developments have made use of diffraction as a contrast mechanism, in order that the grains (DCT, 3DXRD) or chemical composition or crystallographic phases (diffraction or fluorescence tomography) can be mapped in 3D (Poulsen, 2004; Johnson *et al.*, 2008; and Bleuet *et al.*, 2008).

The PSICHE beam line has the highest energy spectrum at SOLEIL, with a peak flux at around 25 keV, and useful flux at energies above 80 keV. The beam line performs two main types of experiments. The principal applications are the study of samples at extreme pressures using diffraction, and materials science investigations using tomography and radiography. The tomography instrument, which will be presented in this article, has been designed and optimised for *in situ* material science, although it is not restricted to these applications. Imaging can be performed across a range of sample sizes and spatial resolutions, and monochromatic and filtered white beam (polychromatic) illumination can be used. The high-pressure measurements use powder diffraction techniques to measure crystallographic parameters (either monochromatic beam, angular dispersive diffraction with 2D detectors, or white beam, energy dispersive diffraction with a germanium detector). The multi purpose nature of the beam line has led to the development of a very flexible instrument, and one which is particularly well suited to combining imaging and diffraction techniques. In particular, imaging and diffraction can be combined in both monochromatic and polychromatic schemes.

II. INSTRUMENT

The tomography instrument consists of the x-ray optics, which are shared with the diffraction activity of the beamline, the mechanical stages of the tomograph, the detector system, and the instrument control and data analysis systems. Parallel beam synchrotron tomography is a maturing technique, so aspects of the design are based on existing equipment at other facilities (Wang *et al.*, 2001; Stampanoni *et al.*, 2006; Boller *et al.*, 2010; and Drakopoulos *et al.*, 2015). However, the PSICHE instrument offers multiple developments with respect to existing systems. The instrument will be briefly presented here, followed by a section in which the new or innovative aspects of the design will be discussed in more detail.

A. X-ray optics

The SOLEIL storage ring operates at an energy of 2.75 GeV, with a stored current of 450 mA, which will soon be upgraded to 500 mA. The storage ring operates in top up mode, so there are only minimal variations in current as a function of time. The PSICHE beam line is equipped with an in-vacuum, 2.1 T wiggler insertion device (Guignot *et al.*, 2013). A wiggler source was chosen for two reasons: Firstly, to provide the highest possible photon energies from the SOLEIL storage ring, in order to have sufficient transmission through large or dense samples or sample assemblies, and secondly, to give a continuous energy spectrum suitable for energy dispersive diffraction measurements (a technique perfectly suited to high pressure *in situ* measurements where the angular opening around the sample can be extremely limited). The maximum beam size is around 15×4.5 mm^2. By using a half–object acquisition strategy for tomography (360° rotation of the sample, with the rotation axis placed off-centre with respect to the detector (Kyrieleis *et al.*, 2009)) the horizontal field of view can be doubled; hence the maximum sample diameter (without working in local tomography) is around 25-30 mm. The main x-ray optics are shown schematically in Figure 1. After the front end aperture, the first elements are a series of fixed attenuating filters (chemical vapour deposition diamond and silicon carbide), which absorb the low energies from the source. These absorb approximately 75% of the total 1800 W power accepted by the front end aperture (Moreno, 2015). After these absorbers, the peak flux of the energy spectrum is at around 22 keV. The beam is then defined by primary slits. Next is a dynamically bendable x-ray mirror, which can be used as a low-pass energy filter, and to vertically focus the beam. A fixed exit, double crystal monochromator with silicon (111) and (311) crystals can be used to select narrow

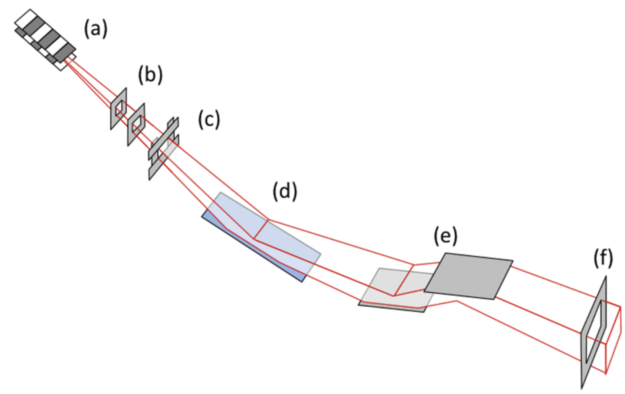

FIG. 1. Beam line optics schematic. (a) In-vacuum wiggler, 0 m. (b) Fixed CVD and SiC absorbers 16.5-17.5 m. (c) Primary slits, 17.5 m. (d) Dynamically bendable vertically focusing mirror, 18.5 m. (e) Bragg-Bragg monochromator, 20.5 m. (f) Optional additional filter support, 21 m. Elements d-f can be individually removed from the beam.

bandwidth monochromatic radiation ($\Delta E/E \sim 1.3 \times 10^{-4}$) for dose sensitive samples or for diffraction contrast imaging. Finally, further filters can be mounted on an additional water-cooled support. All x-ray optics after the primary slits are optional, and can be removed from the beam. For imaging either monochromatic or filtered white beam radiation may be used, according to the requirements of the experiment. The beam flux at the sample position is around 3×10^{11} photons s^{-1} mm^{-2} at 25 keV in monochromatic mode. The white beam power with only the permanently fixed absorbers is around 13 W mm^{-2}, or 2×10^{15} photons s^{-1} mm^{-2}. This is more than sufficient to damage most samples and the detector, so the beam must be further filtered using the x-ray mirror and additional filters. Typical exposure times are given in Section II C, and filtering strategies are discussed further in Section II E. Vertical focusing using the x-ray mirror can be applied to both white and monochromatic beams to increase the flux density.

B. Tomograph stages

The tomograph is based on a high precision, high load capacity RT500 rotation stage and linear translation from LAB Motion Systems (Figure 2). The rotation stage has a measured eccentricity better than 150 nm. The load capacity

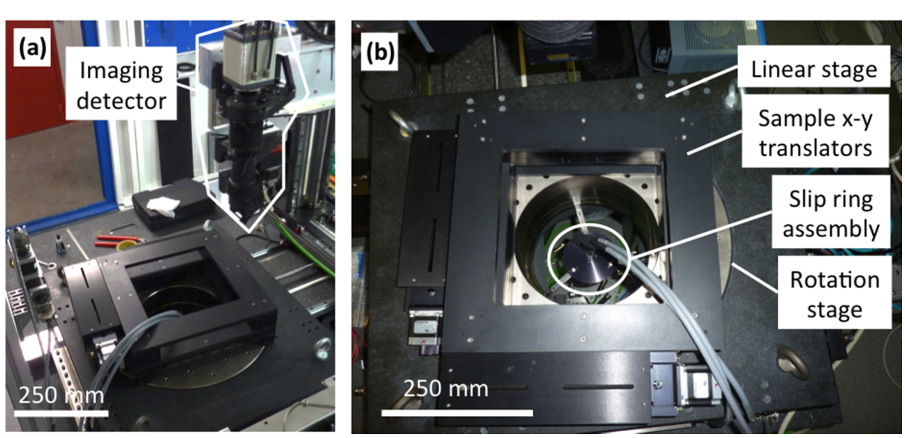

FIG. 2. The PSICHE tomography instrument. (a) Tomograph and detector. (b) View of the open aperture in the rotation stage. The slip ring can be removed if more space is required.

of the rotation stage is limited to around 50 kg by the sample translators, allowing the largest sample environments to be installed while maintaining sub-micron spatial resolution. The rotation stage is mounted on a linear translation system to remove the sample from the beam for taking reference images. The resolution of this motor is <50 nm, allowing precise repositioning of the rotation axis (Stampanoni *et al.*, 2006). All elements of the tomograph including the granite table feature an open aperture of at least 250 mm to allow large samples or sample environments to be installed inside the tomograph, below the sample position. The sample translators can be connected using a slip ring system to allow continuous rotation unrestricted by cables. If this slip ring is removed, then the vertical space available for samples below the beam height is either 1400 mm (monochromatic hutch) or 840 mm (white/pink beam hutch).

C. Detector

The detector system, visible in Figure 2(a), uses a sensor coupled to a scintillator screen by visible light objectives. The system is white beam and high energy compatible in that the lenses and sensor are positioned out of the path of the primary x-ray beam. The detector is designed to be modular, so that components can be easily exchanged in order to optimize the configuration, replace damaged elements, or to allow the system to evolve by incorporating new components. The efficiency of the system has been modeled following the approach described in Desjardins *et al.* (2014), allowing exposure times to be simulated for all combinations of x-ray and detector optics (Desjardins *et al.*, 2014). The shape of the detector has been optimized to allow the sample to be brought close to the scintillator, and to avoid interference with *in situ* equipment. The front of the detector is as flat as possible, with the scintillator mounted close to the front surface and bottom edge of the detector (<2.5 mm and 12.5 mm, respectively). Scintillators are mounted on interchangeable, tilt adjustable supports. The detector is equipped with a Hamamatsu Orca Flash4.0 sCMOS camera (Hamamatsu, 2016). This has been selected for versatility, allowing full frame rates of up to 100 fps for moderately fast tomography, or exposures of up to 10 s for diffraction contrast tomography experiments. Given a region of interest of 2048×512 pixels for reduced readout time, a full tomography dataset of 2000 radiographs can be recorded in 5 s. The Lima device server allows multiple frames to be accumulated in order to improve the effective dynamic range from the small format sensor (physical pixel size 6.5×6.5 μm^2, full well capacity 30 000 electrons, readout noise 1.5-1.9 electrons RMS (Hamamatsu, 2016)). The optics and camera are installed using Nikon F-mount interfaces, so that most foreseeable equipment can be quickly and reproducibly installed using easily available adaptors. The lens and camera are mounted on independently motorized stages, running on a single set of rails to ensure parallel movement. This allows the system to adapt to different optics, or to make coupled movements of the lens and camera to change the magnification. Currently, optical magnifications between 0.8× and 20× are possible. With the current camera, this results in pixel sizes from 8 μm to 0.325 μm, respectively, with true spatial resolution at the highest magnification of better than 1 μm. In future this range will be extended to 50× optical magnification for a 0.13 μm pixel size, with true resolution of 0.5 μm (Koch *et al.*, 1998 and Stampanoni *et al.*, 2002). With the current detector system equipped with a 50 μm LuAG scintillator and a 10×, 0.28 numerical aperture objective giving an effective pixel size of 0.65 μm and the storage ring in regular 450 mA operation, the resulting exposure time is 450 ms per radiograph in monochromatic mode at 28 keV. In pink beam mode, the same mean energy can be achieved by using the x-ray mirror and aluminium and tin filters (elements D and F, Figure 1). In this case the exposure time can vary between 5 and 200 ms depending on the thickness of the tin (0.4–0.9 mm). Similarly, at 40 keV, the exposure times would be around 1200 ms for monochromatic mode, or between 5 and 1000 ms for filtering with the x-ray mirror and 0.5–2 mm of copper. These options are further discussed in Section II E, and are illustrated in Figure 3.

D. Control and acquisition

Control of the instrument is performed using Spyc, the SOLEIL iPython based command line and scripting environment. This controls Tango devices from an iPython shell. The functionality of the instrument can be extended using macros written in Python language, and using Python libraries to perform calculations. In particular, such functions are used to control the relative positions of the camera and optics in the detector, to move to the nominal focus positions for each optic, avoid collisions, and to change magnification by zooming. Fast data acquisition is performed using FlyScan, developed in-house by SOLEIL to minimize dead time (Leclercq *et al.*, 2015). This acquisition mode uses continuous movement of the rotation axis with hardware synchronisation to the camera. The readout time of the camera is sufficiently small (10 ms per full frame in normal mode) that in most situations it can be considered negligible.

Data treatment and tomographic reconstruction can be performed at the beam line or using the SOLEIL computing cluster. At the beam line, two large capacity disk arrays store raw and treated data, and a GPU server performs reconstructions, allowing first reconstructions to be viewed in near real time, without file transfer or cluster queuing overheads. Currently, PyHST2 is used for reconstruction, offering a range of options useful for synchrotron tomography, and exploit GPU acceleration for fast online processing (Mirone *et al.*, 2014).

E. Innovations

1. Pink beam spectra from a broad-spectrum source

Many synchrotron beam lines use wide bandpass monochromation systems to increase the flux available for a measurement compared to a narrow bandpass double crystal monochromator, while maintaining sufficient monochromaticity that the reconstruction does not exhibit beam-hardening artefacts. Current approaches include multilayer monochromators (Stampanoni *et al.*, 2006 and Boller *et al.*, 2010),

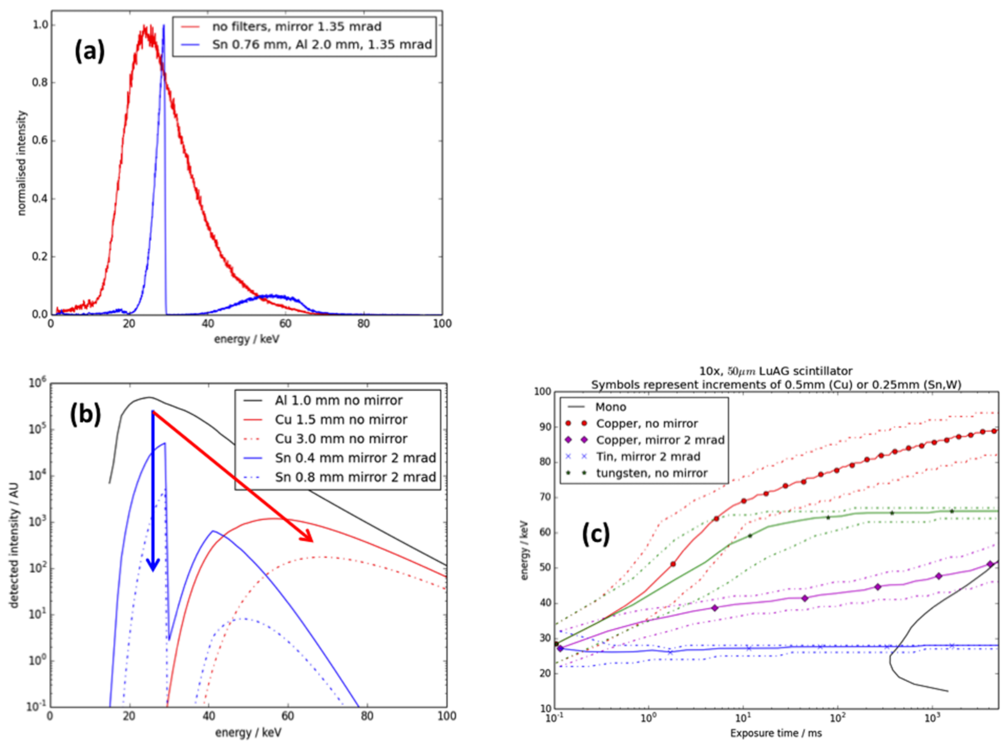

FIG. 3. (a) Measured spectra with and without absorption edge filtering. (b) Effect on the beam spectrum of filtering with copper, and with the x-ray mirror and tin. The first option results in beam hardening (red arrow), while the second option allows the mean energy to be maintained (blue arrow). (c) The beam spectrum plotted against resulting exposure time for different filtering schemes, plus the double crystal monochromator. The beam spectrum is shown by the quartiles and the interquartile mean. Simulated for Hamamatsu ORCA camera, 10× objective, 50 μm scintillator, YAG in (b), LuAG in (c), for normal synchrotron operating conditions.

pinhole monochromators using compound refractive lenses (Vaughan *et al.*, 2011), filtering of undulator (Boller *et al.*, 2010), or wiggler sources (Drakopoulos *et al.*, 2015 and Sanchez *et al.*, 2012). It should be noted that absorption edges in the scintillator (for example lutetium, K-edge 63 keV) can be exploited to define the effective spectrum (Sanchez *et al.*, 2012). A development unique to the PSICHE beam line is the use of the x-ray mirror and filters to produce relatively narrow spectra (typically a few keV full width at half maximum intensity) from the broad spectrum of the wiggler source. The mirror acts as a low pass energy filter, as discussed in (Cloetens, 1999). The mirror has an iridium coating, giving a critical energy of ~86/α keV, where α is the angle of incidence in milliradians. The filters generally act as high pass filters. Materials with suitable x-ray absorption edges (sliver, 25 keV, tin 29.2 keV) can be exploited, in combination with the mirror, to give a more monochromatic result. A water-cooled filter support and sandwich structured filters (for example, aluminium/tin/aluminium) allow low melting point filter materials to be used despite the high beam power. The resulting spectrum can be tuned by adjusting the angle of incidence of the mirror and the thickness and material of the filters. If average energies above ~55 keV are required, then the mirror is removed from the beam and the spectrum is defined using filters only, as described in (Sanchez *et al.*, 2012). An advantage of defining the beam energy with the x-ray mirror and the absorption edges of filters and scintillator is that the flux can be adjusted by adding or removing filters while having relatively little effect of the average energy, thus avoiding the tendency for more filters to harden the beam spectrum, as illustrated in Figure 3(a) (Drakopoulos *et al.*, 2015). This allows effective operation in all filling modes of the storage ring, which can vary between 15 and 450 mA depending on operation mode. Figure 3(b) illustrates the range of beam spectrum versus exposure time that can be accessed via some of these filtering approaches.

2. High load, open aperture stage for in situ devices and tall samples

The PSICHE instrument is currently unique in being the only synchrotron tomography beam line offering a high load capacity rotation stage with a completely open 250 mm diameter aperture in the sample stage (see Figure 2). This allows large *in situ* sample environments to be installed inside the rotation axis (Figure 4(a)). This improves mechanical stability compared to classical designs in which the equipment must be added above the sample, and frees space around the sample, allowing detectors or other equipment to be brought closer. In this example the mass of the *in situ* testing device is around 20 kg, but heavier sample environments can be installed. It allows samples more than 1 m tall to be studied, without being limited by the maximum vertical distance between the beam and the sample stage, as the sample can be installed inside the axis (Figure 6(a)). A further possibility is that a multiple sample changer system could be installed in the space, providing an alternative to robot arm type sample manipulators.

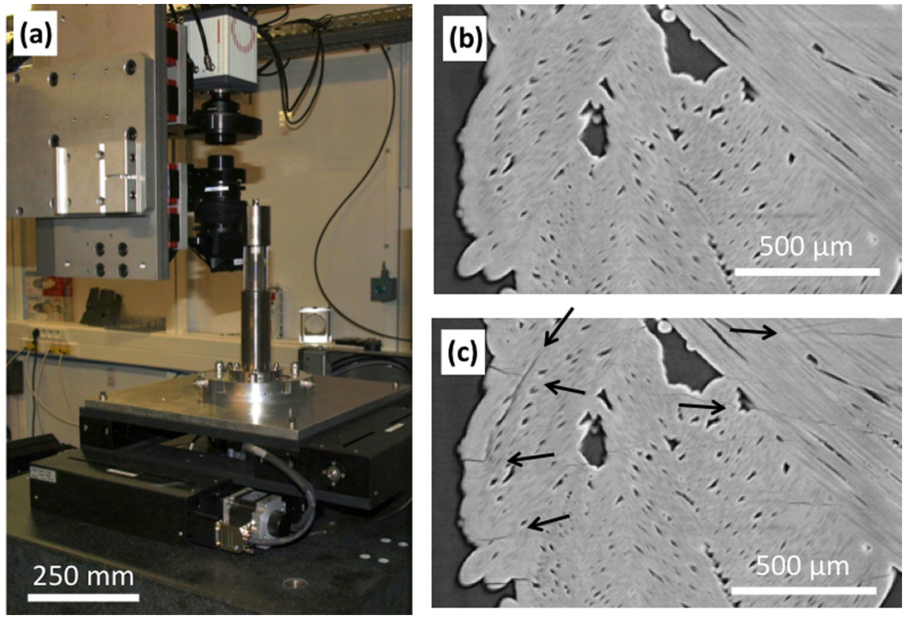

FIG. 4. *In situ* materials testing. (a) The *in situ* loading machine of ENPC installed on the tomograph. Reconstructed sections from the SiC-SiC fibre composite in (b) the initial state, and (c) final loading step before failure showing cracks both perpendicular to the applied load (vertical) and between the fibre plies.

3. *Combining diffraction with tomographic imaging*

The instrument and beam line are designed to allow tomography and imaging to be combined with diffraction in both monochromatic/angular dispersive and polychromatic/energy dispersive modes. The imaging detector can be equipped with an x-ray transparent visible light mirror in order that the diffraction signal from the sample can be collected simultaneously with radiography. The PSICHE beam line is equipped with a combined energy and angular dispersive diffraction detector system (CAESAR, Wang *et al.*, 2004), allowing the 2θ angle of the energy dispersive detector to be varied between 2° and 30° while maintaining a sphere of confusion of 3×6 μm^2. By collecting energy dispersive spectra at a series of angles the reciprocal space coverage can be extended, and high quality, background corrected data acquired efficiently (Wang *et al.*, 2004). Because both the incident and diffracted beams are defined by slits, the signal is acquired only from a gauge volume defined by their intersection. The size of this gauge volume is typically of the order of $20 \times 20 \times 200$ μm^3. The 3D spatial resolution makes this approach a natural complement to tomography. Depending on the alignment of the sample and the detector, different orientations of the diffraction scattering vector can be investigated. The tomography rotation axis can be used to select the orientation of the scattering vector, or can be oscillated to sample a larger selection of grains, depending on the sample and the requirements of the measurement. Furthermore the white beam allows Laue diffraction approaches to be used (Medjoubi *et al.*, 2012).

4. *Radiography for large volume cell high-pressure experiments*

A number of high-pressure experiments use large volume cells (Paris-Edinburgh or multi-anvil systems). In these experiments, the samples are often complex assemblies of multiple components (capsules, thermocouples, heating elements, etc). Radiography is a useful diagnostic for diffraction experiments, greatly assisting in sample alignment, and showing the condition of the sample assembly. For these experiments, the beam is usually focused vertically at the sample position to increase flux. Therefore, images are constructed using a scanning approach. The sample is scanned through the line beam, while a series of images are recorded on the imaging detector. Each image is integrated vertically to produce one line of pixels in a 2D image. The spatial resolution in the vertical direction is given by the beam focus. In some cases, such as molten samples, it may be interesting to measure density from the absorption of the x-ray beam (Katayama *et al.*, 1996 and Malfait *et al.*, 2014). Alternatively, the unfocused beam can be used for faster full field radiography, for example, for falling sphere viscosity measurements (Perrillat *et al.*, 2010).

III. CASE STUDIES

In this section, a number of examples of experiments are given to illustrate the potential of the instrument.

A. *In situ* materials testing

A typical case study for the tomograph is the *in situ* mechanical testing of silicon carbide (SiC) composite tubes. The samples were mounted in a mechanical testing rig developed by the Navier laboratory (ENPC, Paris) shown in Figure 4(a) (Bruchon *et al.*, 2013). This is designed such that the mechanical components are mounted inside the aperture of the rotation stage, as described above. This improves the mechanical stability of the system, and reduces the space required around the sample, allowing the detector to be brought closer. The same machine can be installed at the laboratory microtomograph at ENPC, allowing experiments to be prepared in the laboratory prior to synchrotron beam time. Measurements were made using monochromatic beam radiation, in order to achieve the best image quality and to improve phase contrast (33 keV, 5 μm pixel size, 250 μm LuAG scintillator, 10 frames of 25 ms accumulated per projection, 1500 projections). The total exposure time per scan was around 7 min, although the dead time associated with this measurement was significantly higher, as this experiment was carried out before the implementation of the FlyScan acquisition mode. A similar experiment has recently been successfully tested in FlyScan mode with pink beam illumination, allowing more projections with increased spatial resolution to be acquired in similar scan time (average energy 40 keV, 2.5 μm pixel size, 250 μm LuAG scintillator, 10 frames of 15 ms accumulated per projection, 6000 projections). Figures 4(b) and 4(c) are sections through the reconstruction of the material before and after loading, showing the development of cracks in multiple orientations. These data have been analysed using digital volume correlation (tracking local displacements in order to extract the deformation field) for the study of deformation and failure mechanisms (e.g., Lenoir *et al.*, 2007).

B. Diffraction contrast tomography

Diffraction contrast tomography uses the diffraction spots captured on a high resolution 2D detector placed close to the sample to reconstruct the grain shapes, positions, and crystallographic orientations, in order to reconstruct a 3D grain map (Johnson *et al.*, 2008 and Ludwig *et al.*, 2009). Figure 5 shows a first DCT reconstruction from data collected at the PSICHE beam line as a demonstration of the feasibility of the technique. The DCT analysis and reconstruction software will be installed at SOLEIL in due course. The sample consists of sintered copper spheres (diameter 100 μm). In this case,

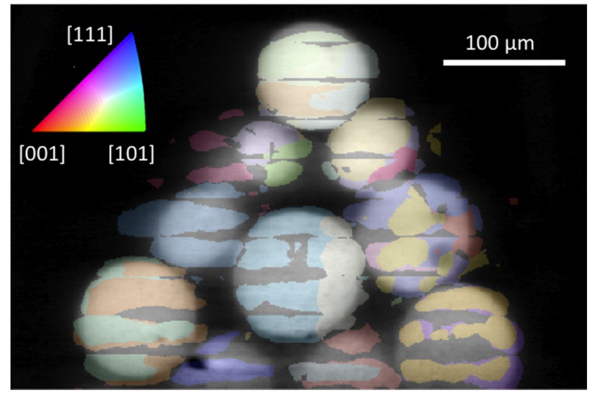

FIG. 5. First diffraction contrast tomography test made at PSICHE. The image shows a section through the grain map overlaid with an absorption contrast reconstruction of the sample morphology. The copper spheres have recrystallized during the sintering process but still contain twin grain boundaries.

the beam was focused vertically to increase flux and reduce the number of grains illuminated. The beamline was used in monochromatic mode, at 40 keV. The effective pixel size was 1.3 μm, with a 90 μm LuAG scintillator. A semi-transparent beamstop was inserted between sample and detector to reduce the intensity of the direct beam image. The exposure time for the diffraction images was 1 s, and in this example 720 images were acquired per scan. A series of scans was acquired, with the sample being translated by 40 μm vertically between acquisitions. Each scan was reconstructed independently and combined to produce the final grain map. The map is shown overlaid with an absorption contrast tomogram of the same volume.

C. Radiation sensitive materials

The tomograph has been used to investigate the effects of drought stress on living plants. The presence of cavitation

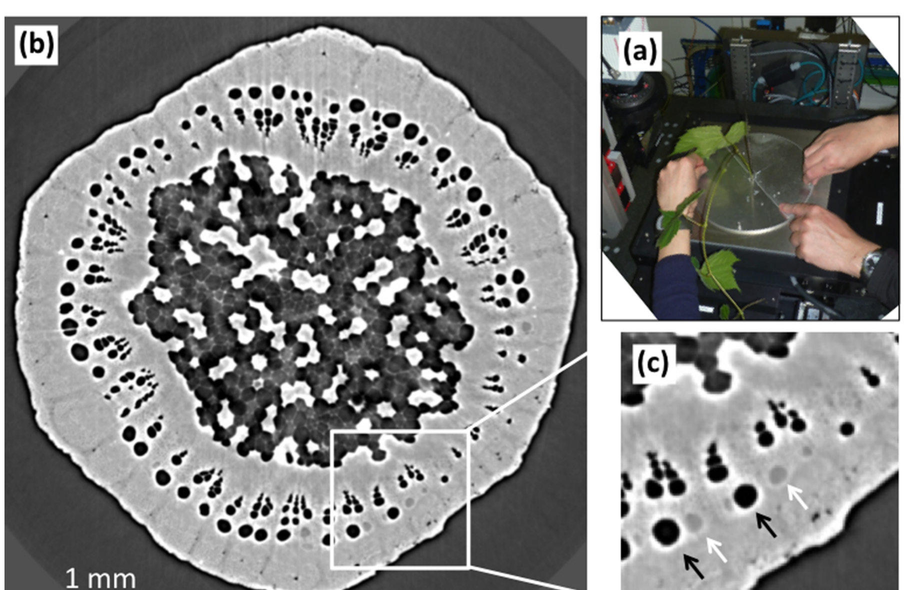

FIG. 6. (a) Study of plants *in vivo*. 1 m tall vine installed inside rotation axis. (b) A reconstructed slice through the stem of a plant showing xylem cavitation. (c) Arrows mark cavitated (dark grey) and full (light grey) vessels on an enlarged region of interest.

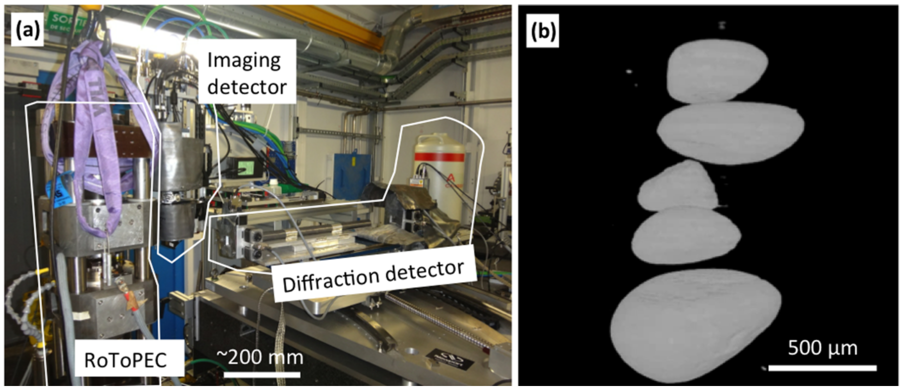

FIG. 7. Tomography and diffraction at extreme pressure. (a) The experiment installed at the beam line. The imaging detector and the energy dispersive diffraction detector are both visible. (b) A 3D rendering from a reconstruction of natural basalt glass beads at high pressure. The small points are contaminants in the pressure-transmitting medium surrounding the beads.

(embolism) in the sap transported by the xylem was determined using phase contrast tomography in monochromatic beam mode (3 μm pixel size, 25 keV, 250 μm LuAG scintillator, 50 ms/frame, 1500 projections). These conditions gave the best imaging quality combined with relatively low radiation dose to minimise beam damage effects. The experiment was made possible by the clear aperture of the rotation stage, which allowed tall plants (>1 m) to be installed inside the stage so that imaging could be carried out near the top of the stems (Figure 6(a)). Here, we demonstrated how high resolution synchrotron tomography allows the direct observation of air and sap-filled xylem conducting elements in the wood of intact plants. It provided non-biased assessment of the ability of plants to adapt to drought conditions. A typical reconstructed section showing the presence of cavitation is shown in Figure 6(b). These findings confirm that microtomography can be used to assess vulnerability to cavitation on intact plants by direct visualization (Choat *et al.*, 2015).

D. Combined imaging and diffraction at extreme pressures

Tomography has also been performed at extreme pressures using the RoToPEC instrument developed by IMPMC, Paris (Philippe *et al.*, 2013 and Le Godec *et al.*, 2016). It consists of a Paris-Edinburgh type high-pressure cell, in which the two anvils are motorized and can be rotated independently about the loading axis. By rotating the anvils together, the sample can be rotated in order to perform *in situ* tomography at pressures up to around 10 GPa. Alternatively, the anvils can be rotated in opposite directions in order to apply a shear strain to the sample. Figure 7(a) shows the RoToPEC installed in the PSICHE white beam hutch. In the current example, the sample studied was a natural basalt glass (Álvarez-Murga *et al.*, 2016). As this is an amorphous material, strain measurement by diffraction is not feasible. By tomographic measurement of the sample volume and density as a function of pressure, the compressibility of the sample can be studied (Lesher *et al.*, 2009). Imaging was performed using the PSICHE tomography detector (2.45 μm pixel size 90 μm LuAG scintillator, 9 ms/frame). Pink beam illumination was produced using the mirror, inclined at 1.8 mrad in order that the critical energy is around 46 keV, and with a 0.8 mm of copper filter to remove low energies. The resulting spectrum had a mean energy of around 44 keV, similar to that shown in Figure 3(b). A tomogram required around 20 min, limited by the rotation speed of the RoToPEC. An image of typical reconstructed data, in which all materials other than the sample have been rendered transparent, is shown in Figure 7(b).

The pressure applied to the sample was measured using energy dispersive x-ray diffraction from the crystalline pressure-transmitting medium around the sample. The pink beam spectrum had sufficient bandwidth that several diffraction peaks could be collected simultaneously.

IV. CONCLUSIONS

This article presents the tomography instrument of the PSICHE beam line, as well as the application of imaging techniques to other experiments performed at the beam line. The instrument is unique in being a synchrotron tomography specifically optimized for the requirements of materials science experiments. The heavy load capacity and large free aperture in the rotation stage and table allow large sample environments for *in situ* studies, with the additional benefit of allowing very tall samples to be studied. The high energies available from the in-vacuum wiggler source allow highly attenuating samples to be measured. The high flux, particularly in pink beam mode, enables time resolved measurements. The beam line uses a range of diffraction techniques in addition to imaging. As a consequence of this, experiments combining imaging with diffraction or other imaging modes (“correlative tomography” (Maire and Withers, 2014)) to reveal more about the behavior or composition of a sample are expected to be an important direction of future development for materials science and also extreme conditions experiments.

ACKNOWLEDGMENTS

Part of the tomograph was funded by ANR project MicroNaSel, No. ANR-10-BLAN-935. The case studies are drawn from the experiments of M. Bornert *et al.*, S. Delzon *et al.*, and J.-P. Perrillat *et al.* DCT data were analysed at the ESRF, Grenoble, France, using the code of W. Ludwig and co-workers. Mario Scheel of the ANATOMIX beam line performed the beam power calorimeter measurements and provided helpful comments on the paper.

Álvarez-Murga, M., Perrillat, J. P., Le Godec, Y., Bergame, F., Philippe, J., King, A., N, Guignot, M, Mezouar, and Hodeau, J. L., "Development of synchrotron X-ray micro-tomography under extreme conditions of pressure and temperature, under review," J. Synchrotron Radiat. (unpublished).

Bertrand, L., Cotte, M., Stampanoni, M., Thoury, M., Marone, F., and Schöder, S., Phys. Rep. **519**(2), 51 (2012).

Bleuet, P., Welcomme, E., Dooryhée, E., Susini, J., Hodeau, J.-L., and Walter, P., Nat. Mater. **7**, 468 (2008).

Boller, E., Tafforeau, P., Ludwig, L., Helfen, L., Weitkamp, T., Salvo, L., Cloetens, P., and Baruchel, J., in *Matériaux 2010, Nantes, France* (2010).

Bruchon, J.-F., Pereira, J.-M., Vandamme, M., Lenoir, N., Delage, P., and Bornert, M., Granular Matter **15**, 783 (2013).

Choat, B., Badel, E., Burlett, R., Delzon, S., Cochard, H., and Jansen, S., Plant Physiol. **170**, 273–282 (2015).

Cloetens, P., "Contribution to phase contrast imaging, reconstruct and tomography with hard synchrotron radiation. Principles, implementation and application," Ph.D. thesis, Vrije Universiteit Brussel, Belgium, 1999.

Cloetens, P., Mache, R., Schlenker, M., and Lerbs-Mache, S., PNAS **103**(39), 14626–14630 (2006).

Cloetens, P., Pateyron-Salomé, M., Buffière, J.-Y., Peix, G., Baruchel, J., Peyrin, F., and Schlenker, M., J. Appl. Phys. **81**(9), 5878 (1997).

Desjardins, K., Bordessoule, M., Petrache, C., Menneglier, C., Dallé, D., Mercere, P., and Medjoubi, K., J. Instrum. **9**, C06001 (2014).

Drakopoulos, M., Connolley, T., Reinhard, C., Atwood, R., Magdysyuk, O., Vo, N., Hart, M., Conner, L., Humphreys, B., Howell, G., Davies, S., Hill, T., Wilkin, G., Pedersen, U., Foster, A., De Maio, N., Basham, M., Yuan, F., and Wanelik, K., J. Synchrotron Rad. **22**, 828–838 (2015).

Guignot, N., Itié, J.-P., Zerbino, P., Delmotte, A., and Moreno, T., "PSICHE: A new beamline dedicated to X-ray diffraction and tomography at pressure at synchrotron SOLEIL," in AGU Fall Meeting Abstracts, 2013.

Johnson, G., King, A., Goncalves Honnicke, M., Marrow, J., and Ludwig, W., J. Appl. Crystallogr. **41**, 310 (2008).

Katayama, Y., Tsuji, K., Kanda, H., Nosaka, H., Yaoita, K., Kikegawa, T., and Shimomura, O., J. Non-Cryst. Solids **205**, 451 (1996).

Koch, A., Raven, C., Spanne, P., and Snigirev, A., J. Opt. Soc. Am. A **15**(7), 1940 (1998).

Kyrieleis, A., Ibison, M., Titarenko, V., and Withers, P. J., Nucl. Instrum. Methods Phys. Res., Sect. A **607**, 677–684 (2009).

Langer, M., Cloetens, P., Guigay, J.-P., and Peyrin, F., Med. Phys. **35**(10), 4556–4566 (2008).

Leclercq, N., Berthault, J., Langlois, F., Le, S., Poirier, S., Bisou, J., Blache, F., Medjoubi, K., and Mocuta, C., "Flyscan: A fast and multi-technique data acquisition platform for the SOLEIL beamlines," in Proceedings of ICALEPCS 2015, Melbourne, Australia, 2015.

Lenoir, N., Bornert, M., Desrues, J., Bésuelle, P., and Viggiani, G., Strain **43**, 193–205 (2007).

Lesher, C. E., Wang, Y., Gaudio, S., Clark, A., Nishiyama, N., and Rivers, M., Phys. Earth Planet. Inter. **175**, 292 (2009).

Lhuissier, P., Scheel, M., Michiel, M. D., Boller, E., Adrien, J., Maire, E., Salvo, L., Blandin, J.-J., and Suery, M., "Ultra fast tomography: New developments for 4D studies in material science," in *1st International Conference on 3D Materials Science*, edited by De Graef, M., Poulsen, H. F., Lewis, A., Simmons, J., and Spanos, G. (John Wiley & Sons, Inc., Hoboken, NJ, USA, 2012).

Ludwig, W., Reischig, P., King, A., Herbig, M., Lauridsen, E. M., Johnson, G., Marrow, T. J., and Buffière, J.-Y., Rev. Sci. Instrum. **80**, 033905 (2009).

Maire, E. and Withers, P. J., Int. Mater. Rev. **59**(1), 1 (2014).

Malfait, W. J., Seifert, R., Petitgirard, S., Mezouar, M., and Sanchez-Valle, C., Earth Planet. Sci. Lett. **393**, 31 (2014).

Medjoubi, K., Thompson, A., Bérar, J.-F., Clemens, J.-C., Delpierre, P., Da Silva, P., Dinkespiler, B., Fourme, R., Gourhant, P., Guimaraes, B., Hustache, S., Idir, M., Itié, J.-P., Legrand, P., Menneglier, C., Mercere, P., Picca, F., and Samama, J.-P., J. Synchrotron Radiat. **19**, 323 (2012).

Mirone, A., Brun, E., Gouillart, E., Tafforeau, P., and Kieffer, J., Nucl. Instrum. Methods Phys. Res., Sect. B **324**, 41 (2014).

Moreno, T., private communication (2015).

Paganin, D., Mayo, S. C., Gureyev, T. E., Miller, P. R., and Wilkins, S. W., J. Microsc. **206**(1), 33 (2002).

Perrillat, J.-P., Mezouar, M., Garbarino, G., and Bauchau, S., High Pressure Res. **30**(3), 415 (2010).

Philippe, J., Le Godec, Y., Bergame, F., and Morand, M., European patent 2984798 (2013).

Philippe, J., Le Godec, Y., Mezouar, M., Berg, M., Bromiley, G., Bergame, F., Perrillat, J.-P., Alvarez-Murga, M., Morand, M., Atwood, R., King, A., and Régnier, S., "Rotating tomography Paris–Edinburgh cell: a novel portable press for micro-tomographic 4-D imaging at extreme pressure/temperature/stress conditions," High Pressure Res. (submitted).

Poulsen, H. F., *Three-Dimensional X-ray Diffraction Microscopy. Mapping Polycrystals and their Dynamics*, Springer Tracts in Modern Physics (Springer, Berlin, 2004).

Rack, A., Scheel, M., Hardy, L., Curfs, C., Bonnin, A., and Reichert, H., J. Synchrotron Radiat. **21**, 815 (2014).

Sanchez, S., Ahlberg, P. E., Trinajstic, K. M., Mirone, A., and Tafforeau, P., Microsc. Microanal. **18**, 1095–1105 (2012).

See http://www.hamamatsu.com/us/en/product/category/5000/5005/C11440-22CU/index.html for Hamamatsu ORCA datasheet retrieved April 2016.

Stampanoni, M., Borchert, G., Wyss, P., Abela, R., Patterson, B., Hunt, S., Vermeulen, D., and Rüegsegger, P., Nucl. Instrum. Methods Phys. Res., Sect. A **491**, 291–301 (2002).

Stampanoni, M., Groso, A., Isenegger, A., Mikuljan, G., Chen, Q., Bertrand, A., Henein, S., Betemps, R., Frommherz, U., Böhler, P., Meister, D., Lange, M., and Alela, R., Proc. SPIE **6318**, 63180M (2006).

Uesugi, K., Takeuchi, A., and Suzuki, Y., "High-definition high-throughput micro-tomography at SPring-8," J. Phys.: Conf. Ser. **186**, 012050 (2009).

Vaughan, G. B. M., Wright, J. P., Bytchkov, A., Rossat, M., Gleyzolle, H., Snigireva, I., and Snigirev, A., J. Synchrotron Radiat. **18**(2), 125–133 (2011).

Wang, Y., De Carlo, F., Mancini, D. C., McNulty, I., Tieman, B., Bresnahan, J., Foster, I., Insley, J., Lane, P., von Laszwski, G., Kesselman, C., Su, M.-H., and Thiebaux, M., Rev. Sci. Instrum. **72**(4), 2062–2068 (2001).

Wang, Y., Uchida, T., Von Dreele, R., Rivers, M. L., Nishiyama, N., Funakoshi, K., Nozawa, A., and Keneko, H., J. Appl. Crystallogr. **37**, 947 (2004).